Cell Reports
Article

Cell PRESS
Open ACCESS

PU.1 Level-Directed Chromatin Structure Remodeling at the *Irf8* Gene Drives Dendritic Cell Commitment

Jörg Schönheit,[1,2] Christiane Kuhl,[1,7] Marie Luise Gebhardt,[1] Francisco Fernández Klett,[3] Pia Riemke,[2] Marina Scheller,[1] Gang Huang,[4] Ronald Naumann,[5] Achim Leutz,[1] Carol Stocking,[6] Josef Priller,[3] Miguel A. Andrade-Navarro,[1] and Frank Rosenbauer[1,2,*]

[1]Max Delbrück Center for Molecular Medicine, 13125 Berlin, Germany
[2]Institute of Molecular Tumor Biology, University of Münster, 48149 Münster, Germany
[3]Department of Neuropsychiatry and Laboratory of Molecular Psychiatry, Charité - Universitätsmedizin Berlin, 10117 Berlin, Germany
[4]Division of Experimental Hematology and Cancer Biology, Cincinnati Children's Hospital Medical Center, Cincinnati, OH 45229, USA
[5]Max Planck Institute of Molecular Cell Biology and Genetics, 01307 Dresden, Germany
[6]Heinrich-Pette-Institute, Leibniz Institute for Experimental Virology, 20251 Hamburg, Germany
[7]Present address: Bristol-Myers Squibb, 80636 Munich, Germany
*Correspondence: frank.rosenbauer@ukmuenster.de
http://dx.doi.org/10.1016/j.celrep.2013.04.007

SUMMARY

Dendritic cells (DCs) are essential regulators of immune responses; however, transcriptional mechanisms that establish DC lineage commitment are poorly defined. Here, we report that the PU.1 transcription factor induces specific remodeling of the higher-order chromatin structure at the interferon regulatory factor 8 (*Irf8*) gene to initiate DC fate choice. An Irf8 reporter mouse enabled us to pinpoint an initial progenitor stage at which DCs separate from other myeloid lineages in the bone marrow. In the absence of Irf8, this progenitor undergoes DC-to-neutrophil reprogramming, indicating that DC commitment requires an active, Irf8-dependent escape from alternative myeloid lineage potential. Mechanistically, myeloid Irf8 expression depends on high PU.1 levels, resulting in local chromosomal looping and activation of a lineage- and developmental-stage-specific *cis*-enhancer. These data delineate PU.1 as a concentration-dependent rheostat of myeloid lineage selection by controlling long-distance contacts between regulatory elements and suggest that specific higher-order chromatin remodeling at the *Irf8* gene determines DC differentiation.

INTRODUCTION

During myelopoiesis, self-renewing hematopoietic stem cells (HSCs) differentiate into broadly myeloid-committed progenitors (common myeloid progenitors [CMPs]), which further differentiate into two major branches: polymorphonuclear phagocytes, comprising granulocytes as well as mast cells, and mononuclear phagocytes, comprising monocytes, macrophages, and dendritic cells (DCs) (Hume, 2008; Geissmann et al., 2010; Liu and Nussenzweig, 2010; Kushwah and Hu, 2011). Although the separation process of granulocytes from monocytes is relatively well studied, it is poorly understood how myeloid precursors specify into DCs. DCs are a heterogeneous cell population with a critical role in immune response and self-tolerance (Steinman and Cohn, 1973; Merad and Manz, 2009). In the current model, DCs are replenished from macrophage-DC progenitors (MDPs) harboring both macrophage and DC potential (Fogg et al., 2006; Geissmann et al., 2010). MDPs are thought to directly yield common DC progenitors (CDPs) (Onai et al., 2007). CDPs are a source of both conventional DCs (cDCs) and plasmacytoitic DCs (pDCs).

A number of transcription factors, such as PU.1, SpiB, Tcf4 (E2-2), Batf3, Id2, and Irf8 (also known as interferon consensus sequence binding protein [ICSBP]) have been implicated in DC development (Watowich and Liu, 2010; Carotta et al., 2010; Schotte et al., 2004; Cisse et al., 2008; Hildner et al., 2008; Hacker et al., 2003). However, it is currently unknown if and how these factors drive the initiation of DC commitment from CMPs. Therefore, we aimed to decipher transcriptional mechanisms initiating DC fate selection. For this purpose, we chose to explore the molecular function and transcriptional regulation of the *Irf8* gene. *Irf8*$^{-/-}$ mice have profoundly depleted pDCs and CD8α^+ cDCs (Tsujimura et al., 2002, 2003b; Ia Sala et al., 2009) but generate more neutrophils and develop a syndrome that resembles human BCR-ABL$^+$ chronic myeloid leukemia (Holtschke et al., 1996; Schiavoni et al., 2002; Tsujimura et al., 2003a; Ginhoux et al., 2009). Moreover, mutations inactivating the IRF8 DNA binding domain have recently been shown to cause human DC immunodeficiency (Hambleton et al., 2011).

Here, we generated Irf8 reporter mice and identified the progenitor stage at which DC lineages separate from alternative myeloid lineages. We show that Irf8 is required for the production of this progenitor and reveal that the initiation of Irf8 expression is controlled by PU.1-induced higher-order chromatin remodeling.

RESULTS

Irf8 Separates the Early DC from Alternative Myeloid Lineage Programs

Irf8$^{-/-}$ mice lack CD8α^+ cDCs and pDCs but maintain normal CD11b$^+$ cDCs, as has been reported previously (Figures S1A

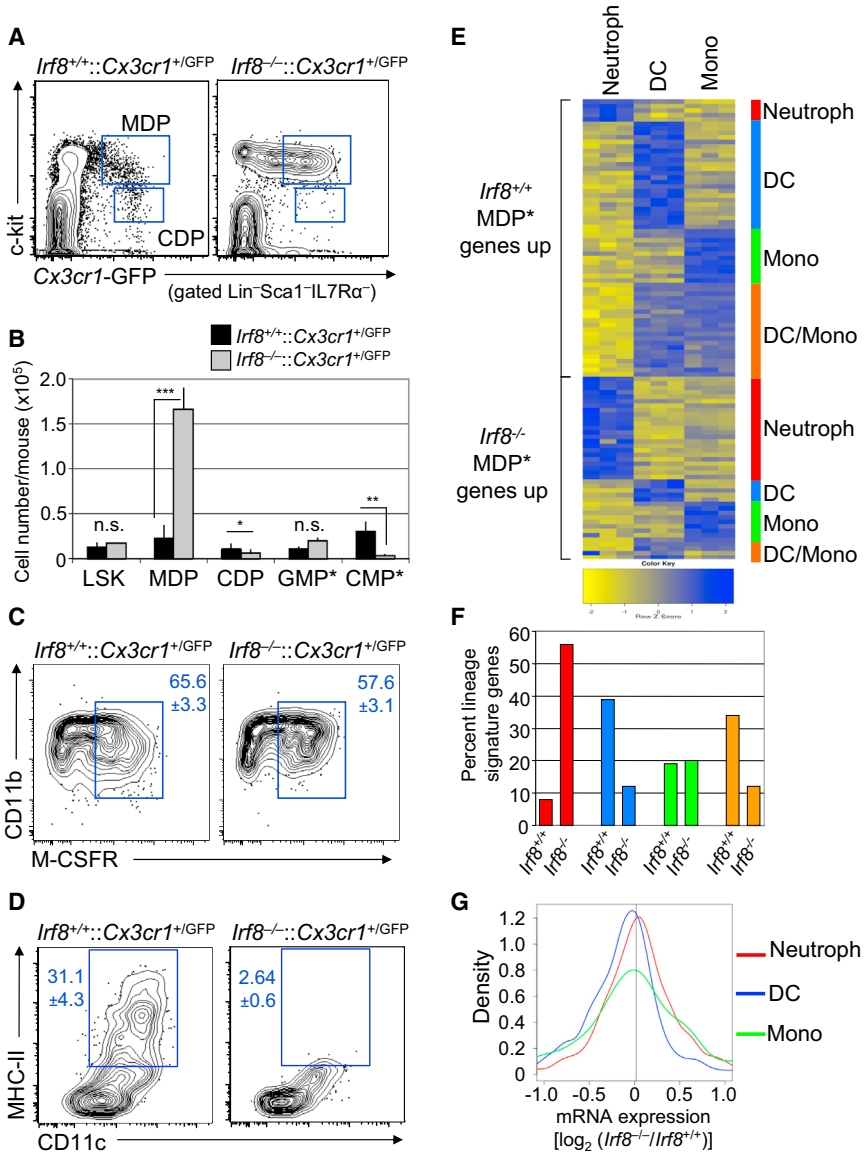

Figure 1. Irf8 Expression Is Required for Transcriptional Identity of Early DC Progenitors

(A) The *Cx3cr1*^{GFP} reporter allele was introduced into the *Irf8*$^{-/-}$ background, and *Cx3cr1*$^{GFP+}$ against c-kit in Lin$^-$Sca-1$^-$IL7Rα^--gated BM cells was analyzed by FACS.

(B) Total numbers of indicated cell populations of *Irf8*$^{+/+}$::*Cx3cr1*$^{GFP/+}$ and *Irf8*$^{-/-}$::*Cx3cr1*$^{GFP/+}$ mice are shown ± SD, n = 3–5 each. LSKs were Lin$^-$Sca1$^+$c-kit$^+$ cells, GMP* were Lin$^-$Sca1$^-$c-kit$^+$CD34$^+$FcγRII/III^{high}*Cx3cr1*-GFP$^-$, CMP* were Lin$^-$Sca1$^-$c-kit$^+$CD34$^+$FcγRII/III^{low}*Cx3cr1*-GFP$^-$.

(C and D) FACS of MDP-derived cells after 7 days in methylcellulose cultures with 10 ng/ml GM-CSF and 40 ng/ml IL-4. We plated 1,000 flow-sorted MDPs and pooled colonies for analysis. *, $p \leq 0.05$; **, $p \leq 0.005$; ***, $p \leq 0.001$; n.s., not significant; n = 3 each.

(E) Heat maps showing downregulated (yellow) or upregulated (blue) genes in MDPs* (Lin$^-$Sca1$^-$IL7Rα^-c-kit^{high}M-CSFR$^+$) of *Irf8*$^{-/-}$ mice. Differentially expressed genes were grouped into DC, neutrophil, monocyte, or shared DC and monocyte signature genes, as indicated by the color code on the right side. For detailed information about signature genes, see Experimental Procedures, Figure S1F, and Tables S1–S5.

(F) Relative distribution of upregulated myeloid signature gene groups in *Irf8*$^{-/-}$ and in *Irf8*$^{+/+}$ MDP*s.

(G) A density plot showing $\log_2$ of fold changes of probe hybridization of *Irf8*$^{-/-}$ versus *Irf8*$^{+/+}$ MDP* progenitors for all DC, neutrophil, and monocyte signature genes. A right shift indicates higher expression in *Irf8*$^{-/-}$ progenitors, and a left shift indicates lower expression.

and S1B) (Tsujimura et al., 2002, 2003b; la Sala et al., 2009). To pinpoint the differentiation stage at which Irf8 is required during DC development, we introduced the *Cx3cr1*^{GFP} reporter into the *Irf8*$^{-/-}$ background, which was shown to mark MDPs as the initiation stage of mononuclear phagocyte commitment (Jung et al., 2000; Fogg et al., 2006). Whereas Lin$^-$/Sca-1$^+$/c-kit$^+$ cells (LSKs) and granulocyte and macrophage progenitors (termed GMPs* in order to indicate that they are *Cx3cr1*$^-$) were normal in *Irf8*$^{-/-}$ mice, CMPs* (also *Cx3cr1*$^-$) and CDPs were reduced (Figures 1A, 1B, and S1C). However, surprisingly, the *Cx3cr1* reporter revealed a profoundly expanded MDP population. We confirmed this expansion by using M-CSFR as a second marker for the identification of MDPs (termed MDPs* in order to distinguish them from *Cx3cr1*$^+$ MDPs) because M-CSFR expression has been shown to overlap with *Cx3cr1*^{GFP} expression (Waskow et al., 2008) (Figure S1D). Next, we explored the functional potential of *Irf8*$^{-/-}$ MDPs by performing in vitro culture experiments. *Irf8*$^{-/-}$ MDPs were unable to produce DCs but gave rise to normal macrophage progeny (Figures 1C, 1D, and S1E).

To address whether Irf8 affects MDP fate by skewing transcriptional lineage programs, we isolated MDPs* from *Irf8*$^{+/+}$ and *Irf8*$^{-/-}$ mice for genome-wide expression profiling. In the *Irf8*$^{-/-}$ progenitors, the expression of 104 genes was increased, and the expression of 117 genes was decreased by more than 2-fold ($p < 0.05$). Unbiased categorization of the differentially expressed genes for different phagocyte lineage-associated gene signatures (Figure S1F and Tables S1–S4) revealed that the *Irf8*$^{+/+}$ progenitors expressed many DC and/or macrophage genes but few neutrophil genes (Figures 1E and 1F). A loss of Irf8 reversed this distribution in that the expression of DC and shared DC and macrophage genes were reduced, but the expression of neutrophil genes was enhanced. Notably, Irf8 deletion had only minimal effects on macrophage gene expression. Moreover, analysis of the expression of the entire signature gene sets within the *Irf8*$^{+/+}$ and *Irf8*$^{-/-}$ progenitors revealed that Irf8 deficiency resulted in an overall weaker expression of the DC signature,

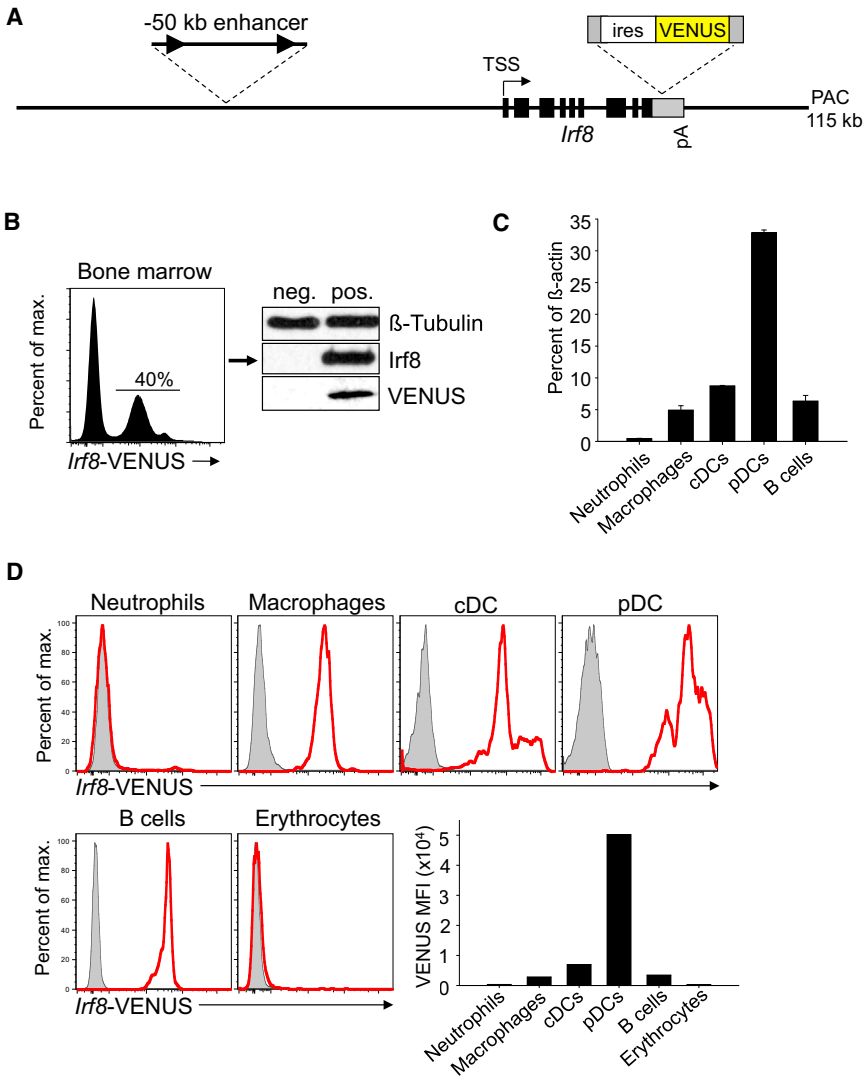

Figure 2. Generation and Validation of *Irf8*-VENUS Reporter Mice

(A) A schematic map of the genomic PAC clone containing base pairs 123,197,900–123,308,928 of murine chromosome 8 (assembly version NCBI37/mm9), which includes the *Irf8* gene. An ires-VENUS cassette was inserted in the *Irf8* 3′ untranslated region and a 2.2 kb fragment containing the −50 kb enhancer was flanked by *lox*P sites (black arrowheads). The *Irf8* gene exon structure (black boxes), the transcription start site (TSS), and the orientation of transcription (arrow) are indicated.

(B) Left, the distribution of VENUS expression in the BM of transgenic mice (line 88). Right, protein from flow-sorted VENUS$^-$ (neg.) and VENUS$^+$ (pos.) fractions were subjected to western blotting and probed with antibodies specific to the indicated proteins.

(C) Quantitative RT-PCR (qRT-PCR) showing mean Irf8 mRNA expression values ± SD in peripheral blood neutrophils (CD11b$^+$Ly6C$^+$M-CSFR$^-$) and B cells (B220+IgM+), and splenic macrophages (CD11b$^+$M-CSFR$^+$), cDCs (CD11c$^+$B220$^-$), and pDCs (CD11c$^+$B220$^+$) all sorted from nontransgenic mice.

(D) VENUS expression in *Irf8*$^{VENUS+}$ transgenic mice (red) and nontransgenic littermates (shaded) derived from line 88. Cell populations were gated as in Figure 2C with the addition of BM erythrocytes (Ter119$^+$). The analysis was performed four times with similar results. Mean fluorescence intensity (MFI) is given for VENUS expression of indicated populations.

See also Figure S2.

a stronger expression of the neutrophil signature, and a largely unchanged expression of the macrophage signature (Figure 1G). Among the Irf8-controlled target genes were transcription factors (e.g., *Klf9*, *Mef2d*, and *Runx2*), chemokine receptors (e.g., *Ccr1* and *Ccr2*), and interferon- and toll-like-receptor-associated genes (e.g., *Ifngr1* and *Ly86*) as well as metalloproteinases (e.g., *Mmp8*) (Table S5).

We conclude that Irf8 is important for MDP transition to the CDP by orchestrating the shift of neutrophil-to-DC gene expression programming. Irf8 deficiency did not change the MDP macrophage program, indicating that Irf8 also acts as a transcriptional separator of the DC from macrophage potential.

Tracing *Irf8* Expression by Generation of Reporter Mice

Because the data showed that Irf8 ablation functionally and transcriptionally separated DC from macrophage potential of MDPs, we reasoned that tracing Irf8 expression at the single-cell level would make the identification of earliest DC-committed progenitors possible. Therefore, we engineered an Irf8 reporter mouse by isolating a phage artificial chromosome (PAC; Mouse PAC Library RPCI-21 296K2) comprising 130 kb of chromosome 8, including all *Irf8* exons with flanking sequences of approximately 81.3 kb 5′ and 28.3 kb 3′. A reporter cassette with an internal ribosomal entry site linked to a VENUS yellow fluorescence marker (ires-VENUS) was inserted into the 3′ untranslated region of *Irf8* exon 9 (Figure 2A), resulting in the expression of a wild-type (WT) Irf8 protein and the VENUS reporter from a bicistronic messenger RNA (mRNA). In addition, we inserted *lox*P sites around a *cis*-regulatory element 50 kb upstream of the *Irf8* transcription start site (see below) to enable its conditional removal from the PAC. We generated stable transgenic lines from three independent founder mice (lines 52, 87, and 88) with complete integration of a structurally intact PAC DNA in two, three, and four copies, respectively (Figures S2A–S2C). Importantly, the PAC transgenes neither enhanced *Irf8* expression over WT levels nor caused any detectable phenotypic abnormalities (Figures S2D and S2E).

Next, we separated bone marrow (BM) cells from the PAC transgenic animals into VENUS$^+$ and VENUS$^-$ fractions using fluorescence-activated cell sorting (FACS) and analyzed Irf8 expression (Figures 2B and S2F). Both Irf8 mRNA and protein

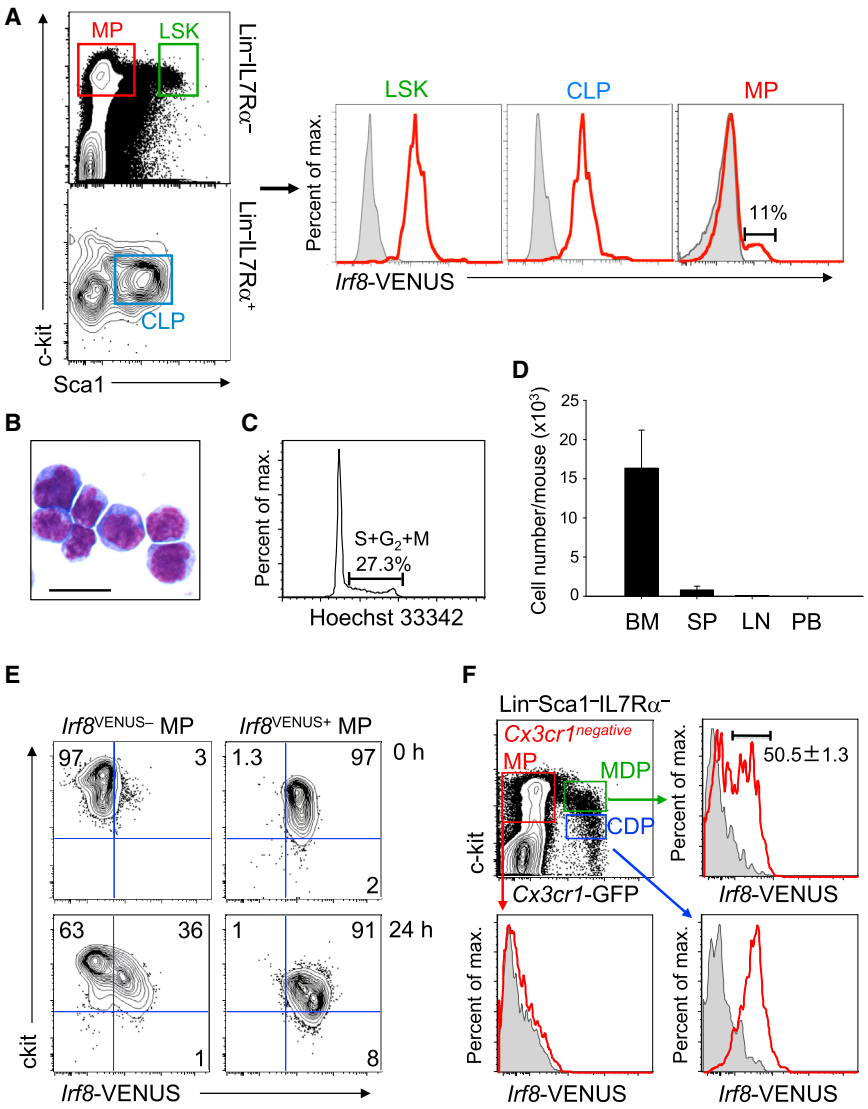

Figure 3. Characterization of *Irf8*$^{VENUS+}$ Myeloid Progenitors

(A) FACS of lineage negative (Lin$^-$) IL7Rα$^-$ (upper left) and Lin$^-$IL7Rα$^+$ (lower left) BM cells of an *Irf8*$^{VENUS+}$ transgenic mouse (line 88). Progenitor populations in the indicated gates were analyzed for VENUS expression. Red histograms represent transgenics, and shaded histograms represent nontransgenic controls. All plots are representative of four mice.

(B–D) Characterization of FACS-sorted *Irf8*$^{VENUS+}$ MPs (Lin$^-$Sca1$^-$IL7Rα$^-$c-kit$^+$*Irf8*-VENUS$^+$).

(B) May-Grunwald-Giemsa stain of *Irf8*$^{VENUS+}$ MPs. The scale bar represents 20 μm.

(C) Analyses of the cell-cycle status of *Irf8*$^{VENUS+}$ MPs.

(D) A representative bar graph indicating the total numbers of flow-gated *Irf8*$^{VENUS+}$ MPs in marrow of long bones (BM), spleen (SP), inguinal lymph nodes (LN), and peripheral blood (PB) of transgenic mice (line 88). Data are represented as mean ± SD.

(E) c-kit versus *Irf8*-VENUS FACS profiling of sorted *Irf8*$^{VENUS-}$ MP (Lin$^-$Sca1$^-$IL7Rα$^-$c-kit$^+$FcγRII/III$^+$*Irf8*-VENUS$^-$) and *Irf8*$^{VENUS+}$ MP (Lin$^-$Sca1$^-$IL7Rα$^-$c-kit$^+$FcγRII/III$^+$*Irf8*-VENUS$^+$) in vitro at 0 hr and 24 hr in the presence of 10 ng/ml IL3, 10 ng/ml IL6, and 50 ng/ml SCF. An FcγRII/III$^+$ gate has been added here to avoid cell-sorting contaminations with LSKs.

See also Figure S3B.

(F) Analysis of *Irf8*-VENUS expression in indicated BM populations from *Cx3cr1*^{GFP}::*Irf8*^{VENUS} double (red histograms) or *Cx3cr1*^{GFP} single transgenic (shaded histograms) mice. Cell gates were Lin$^-$Sca1$^-$IL7Rα$^-$c-kit$^+$*Cx3cr1*$^{GFP-}$ for *Cx3cr1*^{negative} MPs, Lin$^-$Sca1$^-$IL7Rα$^-$c-kit^{high}*Cx3cr1*$^{GFP+}$ for MDPs, and Lin$^-$Sca1$^-$IL7Rα$^-$c-kit^{low}M-CSFR$^+$*Cx3cr1*$^{GFP+}$ for CDPs (Liu et al., 2009). We analyzed three mice of each genotype.

were restricted to VENUS$^+$ cells, indicating that the PAC reported Irf8 expression with high stringency. Moreover, the lineage-specific expression pattern of the VENUS reporter closely paralleled endogenous *Irf8* expression (Figures 2C, 2D, S2G, and S2H). Hence, the reporter mice properly reflected in vivo *Irf8* gene expression.

The *Irf8*^{VENUS} Reporter Marks a Subpopulation of the MDP

Next, we analyzed *Irf8* reporter expression in early hematopoietic precursors. HSCs, multipotent progenitors (MPPs), and common lymphoid progenitors (CLPs) had uniform VENUS levels, indicating that all these cells expressed *Irf8* (Figures 3A and S3A). In contrast, only a small subset of myeloid progenitors (MPs) expressed VENUS (representing ~0.03% of all nucleated BM cells). This subset (designated *Irf8*$^{VENUS+}$ MPs) was comprised of proliferating cells of typical undifferentiated progenitor phenotype that were essentially restricted to the BM (Figures 3B–3D and S3B). *Irf8*$^{VENUS-}$ MPs gave rise to *Irf8*$^{VENUS+}$ MPs in short-term culture assays, but not the other way around, indicating that there is a lineage relationship between both populations, *Irf8*$^{VENUS+}$ MPs being downstream of this relationship (Figure 3E).

Next, we explored the relationship between *Irf8*$^{VENUS+}$ MPs and *Cx3cr1*$^{GFP+}$ MDPs by crossing *Irf8*^{VENUS} with *Cx3cr1*^{GFP} mice. Whereas all *Cx3cr1*$^{GFP-}$ myeloid progenitors were VENUS$^-$ and all *Cx3cr1*$^{GFP+}$ CDPs were VENUS$^+$, approximately half of the *Cx3cr1*$^{GFP+}$ MDP population expressed the VENUS reporter (Figure 3F). Thus, the MDP comprises two subfractions that can be separated on the basis of *Irf8*^{VENUS} expression.

Irf8^{VENUS+} MPs Are Early DC-Restricted Precursors

To evaluate the differentiation potential of *Irf8*$^{VENUS+}$ MPs, we performed transplantation experiments in mice. We injected 25,000 FACS-sorted *Irf8*$^{VENUS+}$ or *Irf8*$^{VENUS-}$ MPs (Figure 4A, S4A, and S4B) or, as a control, 25,000 CDPs (all CD45.2$^+$), into

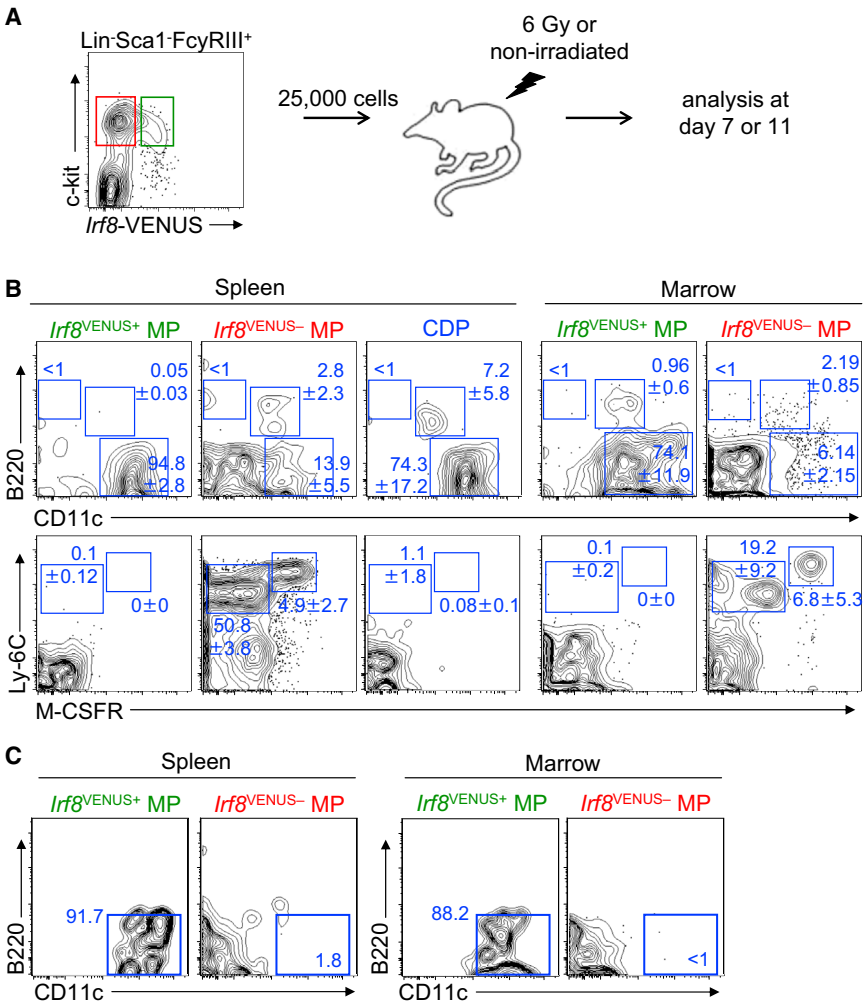

Figure 4. *Irf8*$^{VENUS+}$ Myeloid Progenitors Are Early cDC Precursors

(A) The experimental strategy of myeloid progenitor transplantation. Initial gating of *Irf8*^{VENUS} MPs was extended by gating on FcγRII/III$^+$ cells to avoid cell-sort contamination with HSCs.
See also Figure S3B.

(B) FACS of CD45.2$^+$ donor-derived splenocytes and BM cells 11 days after intravenous transplantation with *Irf8*$^{VENUS+}$ MPs (Lin$^-$Sca1$^-$IL7Rα$^-$c-kit$^+$FcγRII/III$^+$*Irf8*-VENUS$^+$), *Irf8*$^{VENUS-}$ MPs (Lin$^-$Sca1$^-$IL7Rα$^-$c-kit$^+$FcγRII/III$^+$*Irf8*-VENUS$^-$), or CDPs (Lin$^-$Sca1$^-$c-kit^{low}M-CSFR$^+$Flt3$^+$) into sublethally irradiated (6 Gy) recipient mice. Results are representative of five independent experiments for a total number of eight CDP- (average cells per recipient = 500 spleen, 200 BM), 12 each *Irf8*$^{VENUS+}$ MP- (average cells per recipient = 1,000 spleen, 300 BM), or *Irf8*$^{VENUS-}$ MP- (average cells per recipient = 2,000 spleen, 1,000 BM) transplanted mice, respectively. Mean values of at least five mice ± SD are given.

(C) FACS of CD45.2$^+$ donor-derived splenocytes and BM cells 7 days after intravenous transplantation with *Irf8*$^{VENUS+}$ MPs or *Irf8*$^{VENUS-}$ MPs into no irradiated recipient mice.
See also Figure S4.

the tail veins of sublethally irradiated congenic mice (CD45.1$^+$) and analyzed their cellular progeny 11 days posttransplantation. *Irf8*$^{VENUS+}$ MPs gave rise to 1%–2% nucleated cells in the spleens and ~0.3% in the BM of recipients (*Irf8*$^{VENUS-}$ MPs, ~3% in spleens and ~0.9% in BM; CDPs, 0.8% in spleens and 0.1% in BM). In the spleen, we exclusively detected CD11c$^+$MHCII$^+$B220$^-$ cDC progeny of *Irf8*$^{VENUS+}$ MPs, whereas, in the BM, we also found donor-derived CD11c$^+$B220$^+$ pDCs (Figure 4B). *Irf8*$^{VENUS+}$ MPs completely lacked any CD11c$^-$B220$^+$ B cell, Ly6c$^+$M-CSFR$^-$ neutrophil, or Ly6c$^{+/-}$M-CSFR$^+$ monocyte and macrophage potential. *Irf8*$^{VENUS-}$ MPs differentiated into neutrophils, monocytes and macrophages, cDCs and pDCs, but not into B cells. CDPs produced cDCs and pDCs as described before (Onai et al., 2007). Both CD8α$^+$ and CD8α$^-$ pDCs were produced by CDPs and *Irf8*$^{VENUS+}$ MPs at similar frequencies, suggesting that both progenitors are within the same differentiation pathway (Figure S4C). Furthermore, we confirmed a lack of *Irf8*$^{VENUS+}$ MP differentiation potential into macrophages by the absence of F4/80, MOMA-1, MARCO, and SIGNR1 expression on VENUS$^+$ donor-derived splenocytes (Figure S4D). Moreover, we corroborated DC-restricted differentiation potential of *Irf8*$^{VENUS+}$ MPs by transplantation into nonirradiated recipient mice and analysis after 7 days (Figure 4C).

To further determine the DC differentiation potential of *Irf8*$^{VENUS+}$ MPs, we performed in vitro culture experiments in the presence of GM-CSF and FLT3 ligand (FLT3L) for 7 days. Supporting the in vivo results, *Irf8*$^{VENUS+}$ MPs almost exclusively produced CD11c$^+$MHCII$^+$ DCs with a typical spread-out morphology, whereas *Irf8*$^{VENUS-}$ MPs produced much fewer DCs (Figures S4E–S4G).

Altogether, these experiments demonstrated that the *Irf8*^{VENUS} reporter marked an early BM progenitor with exclusive DC differentiation potential.

A Distal Enhancer Drives Myeloid *Irf8* Promoter Activity

The data above indicated that the onset of myeloid *Irf8* expression phenotypically marks and functionally determines the developmental stage of DC lineage selection in the BM. To decipher regulatory mechanisms preceding DC fate choice, we explored how Irf8 expression is initiated. Given that lineage-specific gene expression is primarily orchestrated through gene-distal regulatory elements (Heinz et al., 2010), we computationally identified a number of different evolutionarily conserved noncoding sequences (CNSs) upstream of *Irf8* (Figure 5A).

We performed reporter assays in stably transfected RAW264.7 myeloid cells and NIH 3T3 fibroblasts to test whether these CNSs were able to enhance the activity of the *Irf8* proximal promoter in chromatin context. Both the *Irf8* promoter alone and

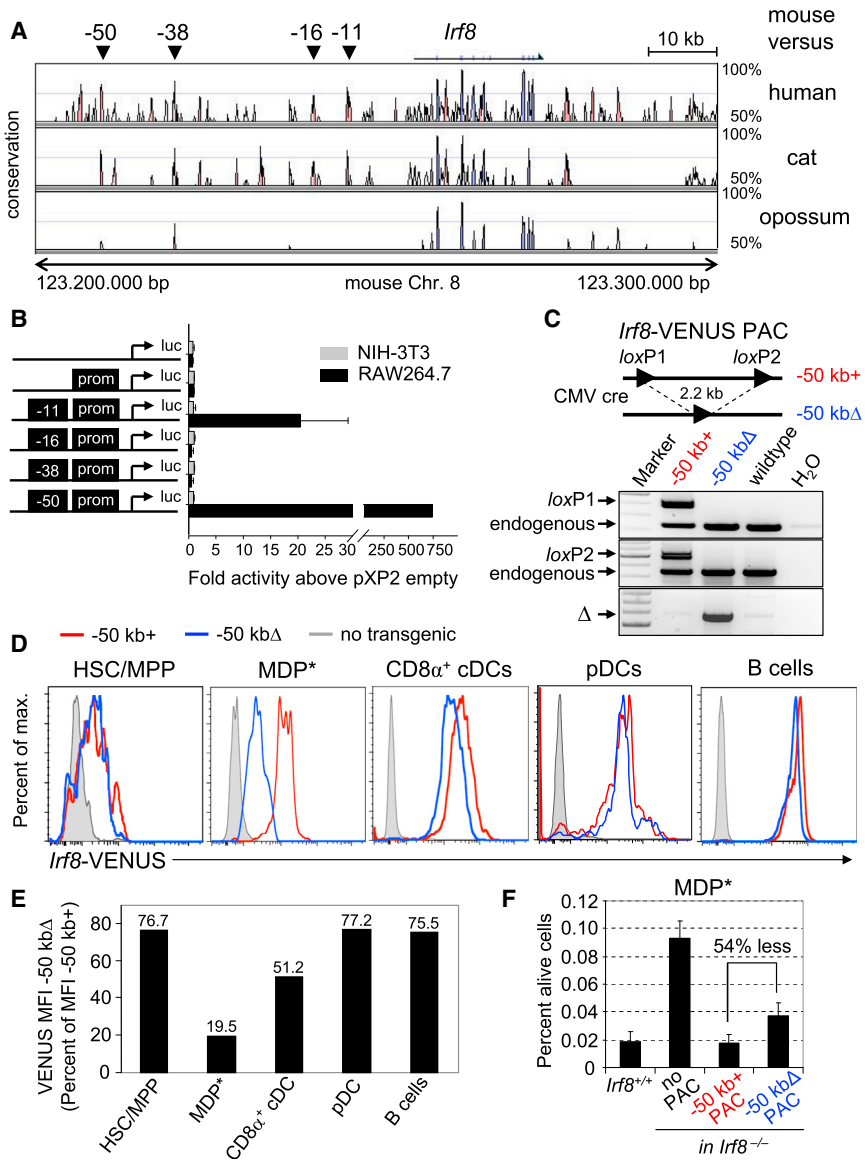

Figure 5. A Specified *cis* Enhancer Drives Irf8 Expression in MDPs

(A) mVista representation (http://genome.lbl.gov/vista/index.shtml) of DNA sequence conservation of the *Irf8* locus. The panels indicate conservation of the mouse genomic region versus the corresponding region in humans, cats, and opossums. Shown are regions of at least 50% conservation (y axis), exons (blue), and noncoding conserved regions (pink). Positions of CNS regions are indicated and labeled on the basis of their distance to the *Irf8* TSS (top).

(B) Shown are pXP2-based luciferase (luc) reporter activities in Irf8-expressing RAW264.7 cells and Irf8-nonexpressing NIH 3T3 fibroblasts stably transfected with the indicated reporter plasmids. Depicted are the mean values ± SD of at least six independent bulks for each construct. The average activity of pXP2-*Irf8*prom-luc was set to 1.

(C) The top panel shows a schematic diagram of the *lox*P-flanked 2.2 kb *Irf8*-VENUS PAC fragment containing the −50 kb enhancer before (+) and after (Δ) its CRE-mediated excision. The bottom panel shows PCR genotyping of tail genomic DNA from the indicated mice (transgenic line 88). PCR reactions with primer pairs detecting the upstream (*lox*P1) or downstream *lox*P site (*lox*P2) before excision, or the fused *lox*P1-*lox*P2 sites (Δ) after excision are depicted.

(D) FACS histograms of the indicated hematopoietic populations from $Irf8^{VENUS-50kb+}$ (red) and $Irf8^{VENU-50kb\Delta}$ (blue) transgenic and nontransgenic (shaded) mice (all from transgenic line 88). HSC and MPP were $Lin^{-}Sca1^{+}c\text{-}kit^{+}$ cells, MDP* were $Lin^{-}IL7R\alpha^{-}Sca1^{-}ckit^{high}M\text{-}CSFR^{+}$, splenic $CD8\alpha^{+}$ cDCs were $CD11c^{+}CD8\alpha^{+}B220^{-}$, pDCs were $CD11c^{+}B220^{+}$, and splenic B cells were $B220^{+}IgM^{+}$. Data are representative of four animals of each genotype.

(E) MFI values of the indicated populations from $Irf8^{VENUS-50kb\Delta}$ mice shown as percentage of $Irf8^{VENUS-50kb+}$ values.

(F) Deletion of the −50 kb enhancer impairs the capacity of the *Irf8* PAC to rescue the DC progenitor phenotype of $Irf8^{-/-}$ mice. MDP* frequencies in BM of $Irf8^{+/+}$, $Irf8^{-/-}$, $Irf8^{-/-}$:$Irf8^{VENUS-50kb+}$, or $Irf8^{-/-}$:$Irf8^{VENUS-50kb\Delta}$ mice. The percentage of living cells per mouse ± SD is given for the indicated population.

See also Figure S5.

the promoter in combination with the −38 kb or −16 kb CNSs were unable to drive reporter gene expression. However, the addition of the −11 kb CNS led to a 20-fold increase in promoter activity in RAW264.7 cells, and the addition of the −50 kb CNS increased the activity 750-fold (Figure 5B). No enhancer function was observed in NIH 3T3 cells.

The −50 kb Enhancer Controls *Irf8* Expression in MDPs In Vivo

Because the −50 kb CNS displayed the highest enhancer activity in vitro, we tested whether this element was required for Irf8 expression in vivo. We modified the $Irf8^{VENUS}$ reporter PAC by flanking a 2.2 kb fragment containing the −50 kb CNS with *lox*P sites and generated transgenic animals (see above). We crossed two of these transgenic lines (87 and 88) with CMV-*cre* deleter animals (Schwenk et al., 1995) to generate a germline deletion of the −50 kb element (designated $Irf8^{VENUS-50kb\Delta}$ mice) (Figure 5C). We confirmed proper excision, copy number maintenance, and genomic integrity of the $Irf8^{VENUS-50kb\Delta}$ transgenes in the resulting offspring (Figures S5A–S5C).

$Irf8^{VENUS-50kb\Delta}$ mice demonstrated a tight cell-type- and developmental-stage-specific requirement of the −50 kb enhancer for *Irf8* expression. Deletion of the −50 kb enhancer decreased VENUS expression only mildly in HSCs and MPPs (both included in the LSK fraction), B cells, and pDCs more strongly in $CD8\alpha^{+}$ cDCs and most profoundly in MDPs* (Figures 5D, 5E, and S5D).

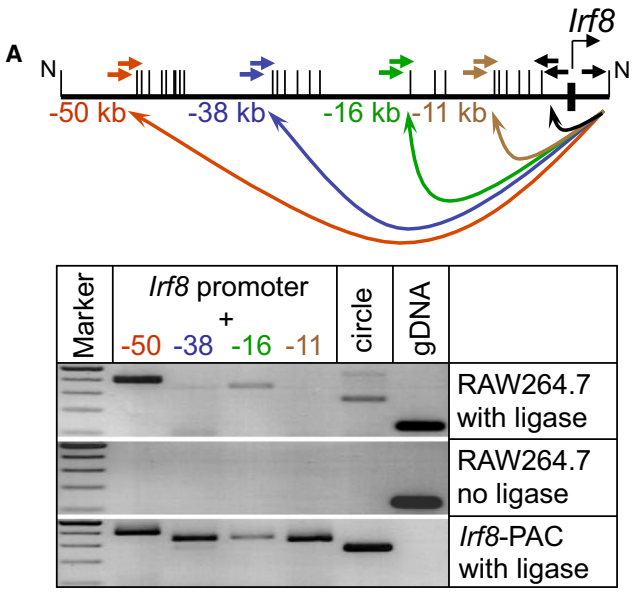

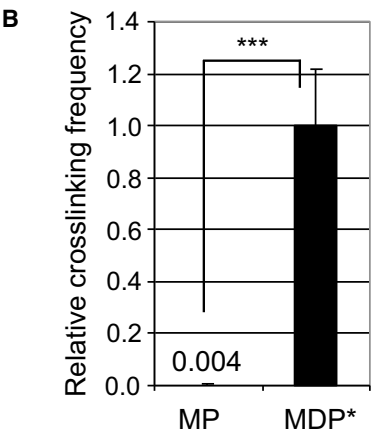

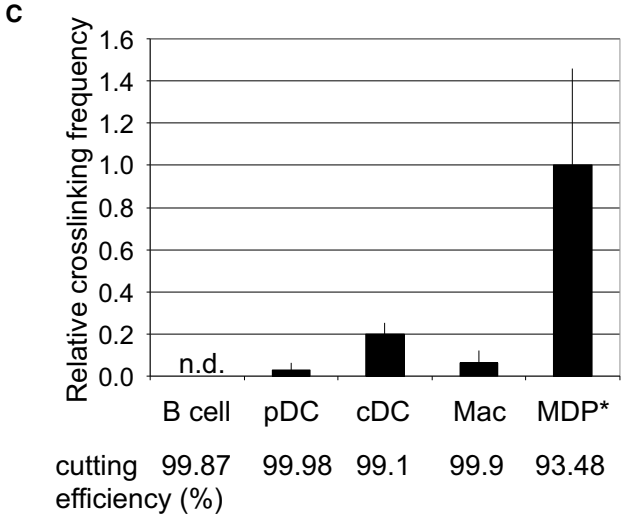

Figure 6. Three-Dimensional Chromatin Structure Remodeling of the *Irf8* Locus

(A) Shown is 3C with RAW264.7 cells. Crosslinked chromatin was digested with *Nco*I (N, each line represents an *Nco*I restriction site) and amplified by nested PCR, as depicted at the top (bold arrows). Nonligated RAW264.7 chromatin served as a negative control, and randomly ligated *Nco*I *Irf8*-PAC fragments were positive controls. PCR amplification of self-ligated *Nco*I *Irf8* promoter chromatin fragments (circle) by two outside-facing primers annealing within the promoter anchor primers served as a digestion and ligation efficiency control. PCR amplification with two primers that annealed within the *Nco*I −50 kb enhancer genomic DNA (gDNA) fragment served as input control.

(B and C) q3C showing −50 kb to *Irf8* promoter spatial proximity in flow-sorted cell populations. All data were normalized to total gDNA content within an *Nco*I restriction fragment. Normalization to looping at the Gapdh locus as housekeeping loop (Spilianakis et al., 2005) gave identical results. No-ligation controls showed no interaction. Data from MDP* was set to 1. All cells were from WT mice. Mean values ± SD are given.

(B) q3C showing −50 kb to *Irf8* promoter spatial proximity in MDP*, but not in M-CSFR$^-$ MPs of the BM. Displayed results are representative for three experiments with similar outcomes. ***, $p \leq 0.001$.

(C) q3C results show cell-type-specific proximity of the −50 kb fragment with the *Irf8* promoter. MDP*s from BM were compared to splenic B cells, pDCs, cDCs, and macrophages. n.d., not detectable.

Next, we explored the functional relevance of the −50 kb element for MDP* formation by introducing the *Irf8*$^{VENUS-50kb+}$ or *Irf8*$^{VENUS-50kb\Delta}$ transgenes into the Irf8-deficient background. Importantly, the *Irf8*$^{VENUS-50kb+}$ transgene completely restored normal *Irf8*$^{-/-}$ MDPs* (Figure 5F). In contrast, the *Irf8*$^{VENUS-50kb\Delta}$ transgene had 54% less efficient restoration capacity.

Altogether, genetic experiments in mice provide in vivo evidence for a specific role of the −50 kb element in the control of Irf8 expression in MDPs.

Higher-Order Chromatin Structure Remodeling at the *Irf8* −50 kb Enhancer

An important question was why the −50 kb enhancer had such a specific effect on Irf8 expression in DC progenitors. We addressed this issue by exploring the higher-order chromatin structure at the *Irf8* locus using chromosomal conformation capturing (3C). First, we screened the *Irf8* upstream CNSs for spatial three-dimensional contacts with the proximal *Irf8* promoter region in RAW264.7 cells. We observed that the −50 kb enhancer and the −16 kb CNS, but not the −38 or −11 kb CNSs, were in spatial proximity with the *Irf8* promoter, thus indicating a specific activating chromatin looping architecture at the *Irf8* locus (Figure 6A).

To corroborate the observation that the −50 kb enhancer-to-*Irf8* promoter contact existed in primary cells, we used a quantitative 3C (q3C) protocol on FACS-sorted cells. Indeed, the −50 kb enhancer was found in physical contact with the *Irf8* promoter in MDPs* but is not found to be in physical contact in MPs (Figure 6B). Moreover, comparison across cell types demonstrated that −50 kb enhancer contact with the *Irf8* promoter was strongest in MDPs* but decreased thereafter in their cDC, macrophage, and pDC progeny and was undetectable in B cells (Figure 6C). Thus, the −50 kb enhancer was brought into physical contact with the *Irf8* gene by tightly controlled remodeling of its higher-order chromatin structure. The dynamics of this remodeling closely paralleled the onset of Irf8 expression during

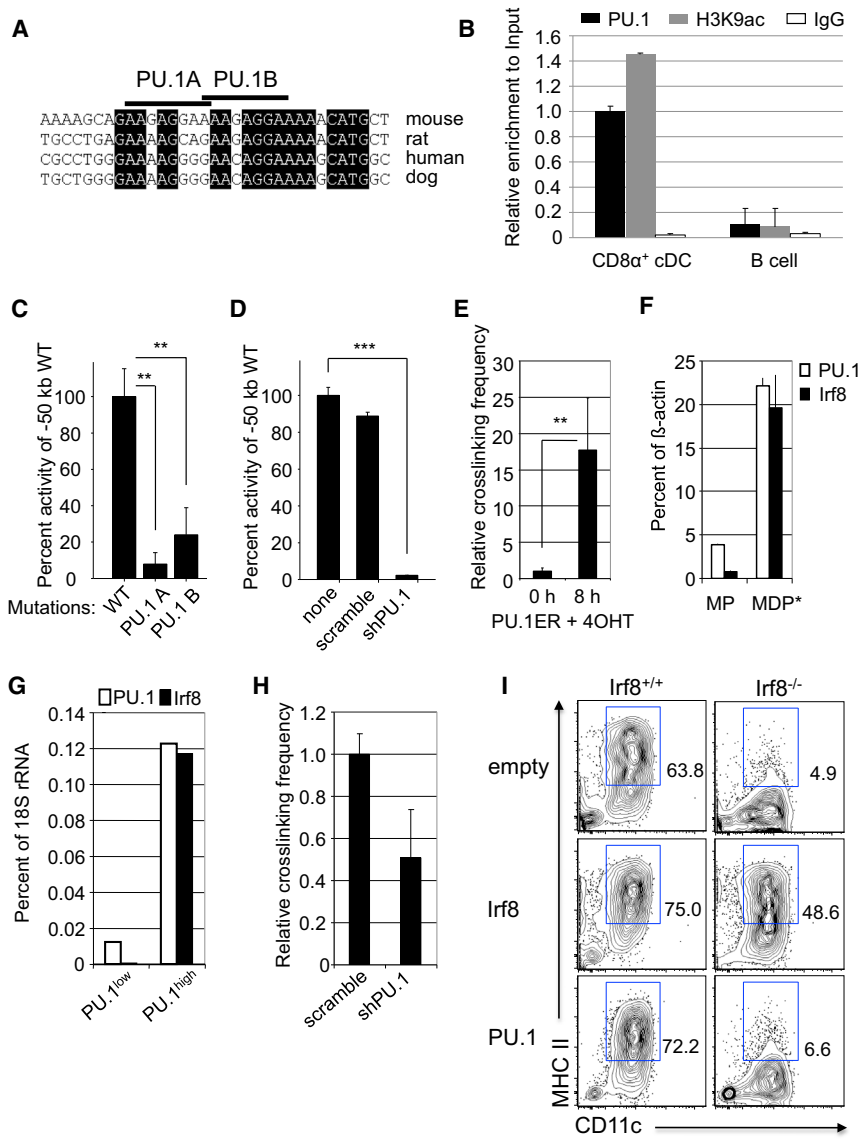

Figure 7. PU.1 Expression Induces −50 kb *Irf8* Enhancer Activity and Chromatin Remodeling

(A) Two adjacent sequence-conserved PU.1 binding motifs are located in the −50 kb element of vertebrates.

(B) The −50 kb element is transcriptionally active and binds PU.1 in cDCs, but not in B cells. ChIP results in the indicated cell types with antibodies recognizing PU.1, acetylated histone H3K9 (H3K9ac), and IgG as control are shown. Specific primers that amplify the −50 kb region by real-time PCR were used. Values normalized to input are given ± SD of three different reactions.

(C and D) Reporter assay in RAW264.7 cells stably transfected with the pXP2-50kb-*Irf8*prom-luc luciferase construct are shown.

(C) Luciferase constructs were carrying mutations in the PU.1 binding sites (GGAA to GCGC) of the −50 kb fragment. Shown are the mean values ± SD of at least six different cell clones for each construct, p = 0.001 (PU.1A) and p = 0.005 (PU.1B). Activity of the nonmutated construct was set to 100%.

(D) Cells were either mock transfected or transiently transfected with constructs expressing shRNAs against PU.1 or a scramble control, along with a GFP marker to allow flow cytometric sorting of transfected cells. The mock control was set as 100%. The experiment was repeated twice with similar outcomes. Mean values ± SD are given; p = 0.005.

(E) q3C shows increased interaction frequency of the −50 kb fragment with the *Irf8* promoter 8 hr after 4-hydroxytamoxifen (OHT) induction of PU.1 expression in *PU.1*$^{-/-}$ERT-PU.1 cells (PU.1ER). n = 3 experiments with similar outcomes. All data were normalized as in Figure 6B. Interaction in *PU.1*$^{-/-}$ERT-PU.1$^{0\ hr\ induced}$ was set to 1. Mean values ± SD are given; p = 0.003.

(F) qRT-PCR of Irf8 and PU.1 messenger RNA (mRNA) expression in FACS-sorted MPs and MDPs* gated as in Figure 6B. Displayed are the mean values ± SD of two biological replicates each.

(G) qRT-PCR of Irf8 and PU.1 mRNA expression in FACS sorted Lin$^-$Sca1$^-$c-kit$^+$ myeloid progenitors isolated from the BM of mice with a deleted upstream regulatory element (URE) of the *PU.1* gene (Rosenbauer et al., 2004).

(H) Impaired q3C interaction frequency of the −50 kb fragment with the *Irf8* promoter in PU.1-shRNA-transfected versus scramble-transfected RAW264.7 cells. Displayed results are representative for two experiments with similar outcomes. All data were normalized as in Figure 6B. The value of RAW264.7^{scramle} was set to 1. Mean values ± SD are given.

(I) Relative distribution of CD11c$^+$MHCII$^+$ cells derived from *Irf8*$^{-/-}$ *and Irf8*$^{+/+}$ c-kit$^+$ BM cells transduced with retroviruses expressing GFP alone, Irf8-GFP, or PU.1-GFP. Cells were kept in liquid culture for 8 days with 100 ng/ml Flt3L and were gated on GFP-expressing cells for analysis. n = 3 replicates per condition were analyzed.

**, p ≤ 0.005 and ***, p ≤ 0.001.

myeloid differentiation and, thus, provided an explanation for the specific effect of −50 kb enhancer deletion on DC progenitors in mice.

PU.1 Binding Is Necessary for −50 kb Enhancer Activity and Induces Chromatin Remodeling

A computational motif search identified two directly adjacent PU.1-binding consensus motifs that were highly conserved among vertebrate species (Figure 7A). Indeed, PU.1 occupied these sites in primary DCs but did not occupy these sites in B cells (Figure 7B). PU.1 occupancy was associated with cell-type-specific H3K9 acetylation, indicating a transcriptional regulatory activity of the −50 kb element in DCs. In the RAW264.7 cell-line model, mutations in either one of these PU.1-binding sites or knockdown of PU.1 by small hairpin RNA (shRNA) diminished −50 kb enhancer activity as well as endogenous Irf8 expression (Figures 7C, 7D, and S6A). Furthermore, activation of a 4-hydroxytamoxifen (OHT)-responsive PU.1-ERT fusion protein in a *PU.1*$^{-/-}$ myeloid progenitor cell line (termed PU.1ER cells) revealed PU.1 as a direct activator of Irf8 expression (Figures S6B–S6D).

To investigate whether PU.1 controls chromatin looping of the −50 kb enhancer to the *Irf8* promoter, we performed q3C assays in PU.1ER cells and found that PU.1 induction rapidly led to a marked increase in looping frequency (Figure 7E).

−50 kb Enhancer Chromatin Structure Remodeling Requires a High PU.1 Level

Intriguingly, although the expression of both Irf8 and PU.1 increased to similar levels in MDPs*, the expression of Irf8 was absent in MPs, whereas the expression of PU.1 was low but readily detectable in MPs (Figure 7F), suggesting that high PU.1 levels are required to trigger Irf8 transcription. To directly test this, we quantified Irf8 expression in myeloid progenitors from PU.1 hypomorphic mice that expressed PU.1 at a 5-fold lower level than the corresponding WT cells (Rosenbauer et al., 2004). Indeed, these progenitors showed almost a complete lack of Irf8 transcripts, indicating that the reduced PU.1 level provided by the hypomorphic alleles was insufficient for Irf8 expression (Figure 7G). In line with this, shRNA-mediated gradual reduction of PU.1 levels in the RAW264.7 model impaired −50 kb enhancer-to-*Irf8* promoter contact formation (Figure 7H). Altogether, these data indicate that PU.1 can function as a concentration-dependent trigger of Irf8 chromatin remodeling and transcription.

PU.1 Fails to Drive DC Differentiation in the Absence of Irf8

PU.1 is known to induce DC differentiation (Carotta et al., 2010; Guerriero et al., 2000). To test whether PU.1 requires Irf8 to induce DC development, we transduced c-kit$^+$ BM progenitors from *Irf8*$^{-/-}$ mice with retroviruses expressing either PU.1 or Irf8 along with GFP from bicistronic mRNAs or with a retrovirus expressing GFP only. GFP$^+$ cells were sorted and cultured with Flt3L to support generation of DCs. Ectopic PU.1 failed to drive development of MHCII$^+$CD11c$^+$Sirpα^-B220$^-$ cDCs and MHCII$^+$CD11c$^+$B220$^+$ pDCs of *Irf8*$^{-/-}$ progenitors, whereas Irf8 restoration rescued the capacity to produce both DC populations (Figures 7I, S6E, and S6F). This result indicates that PU.1 requires the presence of Irf8 to induce DC differentiation.

DISCUSSION

DCs are related to, but clearly distinct from, macrophages (Merad and Manz, 2009; Geissmann et al., 2010), and the identification of cellular precursors of the DC lineage has been the focus of intense research (Ginhoux et al., 2009; Fogg et al., 2006; Manz et al., 2001; Carotta et al., 2010; Liu et al., 2009; Waskow et al., 2008). Taking advantage of a newly generated Irf8 reporter mouse, we report a distinct Irf8-expressing subfraction of the MDP (Fogg et al., 2006). This *Irf8*$^{VENUS+}$ population had the exclusive capacity to differentiate into DCs, but not into monocytes or macrophages, in vivo. Although the cDC potential of *Irf8*$^{VENUS+}$ MPs was strong, the pDC potential was weaker than that of CDPs. One likely explanation for this difference could be that *Irf8*$^{VENUS+}$ MPs require more time than CDPs to fully replenish pDCs. This, along with their higher c-kit level, supports the idea that *Irf8*$^{VENUS+}$ MPs reside upstream of CDPs. However, the question of whether *Irf8*$^{VENUS+}$ MPs are a separate population or whether they overlap with the earliest CDPs requires further investigation. In any case, the identification of *Irf8*$^{VENUS+}$ MPs as an initial DC precursor within the formerly identified MDP population is instrumental in deciphering the earliest molecular events initiating DC development.

Irf8-reporter-based marking of this early DC stage is associated with functional Irf8 dependency in the production of DC progenitors. MDPs isolated from *Irf8*$^{-/-}$ mice had maintained macrophage and monocyte differentiation capacity but completely lacked DC potential in vitro. A recent study suggested that Irf8 is required for the production of DC progenitors and for the restriction of GMP expansion (Becker et al., 2012). By introducing the *Cx3cr1*^{GFP} reporter into *Irf8*$^{-/-}$ mice, we revealed that Irf8 deficiency reduced DC development by impairing the transition of MDPs into CDPs. In contrast, GMPs were not affected. The early differentiation block in *Irf8*$^{-/-}$ mice appears surprising, given that not all DC populations are absent in these animals. However, our data showed that some progenitors can transit into the CDP stage even in the absence of Irf8. These cells may be biased to replenish certain DCs. Alternatively; Becker et al. (2012) have shown that *Irf8*$^{-/-}$ progenitors are less able to replenish all DC populations in chimeric mice, suggesting that homeostatic proliferation may also contribute to the maintenance of CD11b$^+$ DCs in Irf8-deficient animals.

Irf8$^{-/-}$ MDPs showed a lower expression of DC-associated genes but a higher expression of neutrophil-associated genes and an unchanged expression of macrophage-associated genes. This finding indicated that the initiation of DC differentiation choice requires an active, Irf8-dependent shift from neutrophil-to-DC gene expression in MDPs. In light of these data, it appears most likely that the excessive production of neutrophils leading to the development of granulocytic leukemia in *Irf8*$^{-/-}$ mice may be the result of this DC-to-neutrophil "conversion" of the MDP. It will be interesting to see whether a similar mechanism also underlies the development of *IRF8*-mutated human DC immunodeficiency, which can be accompanied by high neutrophil counts as well (Hambleton et al., 2011).

A chromatin-based mechanism driving the molecular commitment of early myeloid progenitors toward DC differentiation has remained elusive. Here, we were able to pinpoint a region located 50 kb upstream of the *Irf8* gene as the major enhancer driving Irf8 expression during DC progenitor formation in vivo. Deletion of the −50 kb enhancer from the engineered *Irf8* PAC led to reduced reporter gene expression in MDPs, but not in stem cells, pDCs, or B cells. Accordingly, DC progenitor development was impaired in the absence of the −50 kb enhancer.

Different models of how distal regulatory elements communicate with proximal gene regulatory regions have been proposed (Wittkopp and Kalay, 2012; Bulger and Groudine, 2011). One of these models suggests that enhancers are placed in physical proximity to promoters through chromosomal looping (Heermann, 2011). Indeed, on the basis of 3C technology, there are now a number of examples known that support the looping model (Palstra et al., 2003; Tolhuis et al., 2002; Apostolou and Thanos, 2008; Spilianakis et al., 2005; Ling et al., 2006). We found that looping of the −50 kb enhancer to the *Irf8* promoter occurred with high specificity with regard to the lineage and developmental stage and, at least in a cell-line model, required

PU.1 as a coordinator. Although it is not yet clear whether PU.1 controls Irf8 chromatin looping directly, our findings suggest a concentration-dependent model in which high PU.1 amounts are required to drive *Irf8* locus looping and transcription. Such a model is supported by the recent finding that high PU.1 levels are also needed to drive Flt3 expression in cDC progenitors (Carotta et al., 2010). Although our retroviral transduction assays have shown that PU.1 requires Irf8 as a downstream target to drive DC development, Irf8 could not substitute PU.1 in DC differentiation (see Figure 7A) (data not shown). Again, this is similar to the inability of Flt3 to rescue PU.1-deficient DC production (Carotta et al., 2010). Altogether, these results suggest that PU.1 controls multiple independently acting molecular pathways to drive DC development. This idea is supported by our results showing that PU.1 controls Flt3 expression independently of Irf8 (data not shown).

In summary, we have isolated an initial Irf8^{+} DC progenitor. In this progenitor, Irf8 transcriptionally organizes the separation of the DC program from that of other myeloid lineages, including the monocytic program. PU.1 induces Irf8 expression by remodelling its higher-order chromatin configuration to loop a distant *cis*-enhancer into physical proximity to the *Irf8* promoter.

EXPERIMENTAL PROCEDURES

Mice and Cell Lines

All mice in this research were studied on a C57Bl/6 background. C57Bl/6 wild-type mice were from Charles River Laboratories. *Irf8*$^{-/-}$ and URE$^{-/-}$ mice were generated as described before (Holtschke et al., 1996; Rosenbauer et al., 2004). *Irf8*^{VENUS} PAC reporter mice were generated by pronuclear injection of the engineered murine *Irf8*-PAC (Figure S1A) into WT C57Bl/6 fertilized oocytes. Injection was conducted at the Max Planck Institute of Molecular Cell Biology and Genetics. PAC^{+} animals were identified by FACS and PCR (primers are available on request). Three independent PAC lines were established and used for this study. Two of these lines were bred to CMV-*Cre* deleter mice (Su et al., 2002), leading to the excision of the *lox*P-flanked −50 kb element. All mouse experiments were approved by the local authorities according to the German Federal Animal Protection Act. RAW264.7, NIH 3T3, 416B, *PU.1*$^{-/-}$ERT-PU.1, and *PU.1*$^{-/-}$ cell lines were cultured as described before (Leddin et al., 2011; Walsh et al., 2002).

Flow Cytometry and Cell Sorting

Single-cell suspensions from indicated organs were analyzed by flow cytometry on a BD LSRFortessa cell analyzer (BD Biosciences). Cell sorting was performed on a FACSAria (BD Biosciences) equipped with an UV laser. Prior to flow sorting of BM precursors, lineage-associated cells were manually depleted after being incubated with CD3, CD4, CD8α, B220, CD19, CD11b, CD11c, and/or Gr-1. Nonspecific binding was reduced where applicable by preincubation with unconjugated antibody to FcγRII/III (2.4G2). Propidium iodide was used for the exclusion of dead cells. Cell-cycle status was determined by staining with Hoechst 33342 stain according to standard protocols.

In Vitro Colony-Forming Assays

Flow-sorted cells (1 × 10^{3}) were seeded in MethoCult (M3234, STEMCELL Technologies) in triplicate. Supplements were treated with M-CSF (10 ng/ml) alone or a cocktail of SCF (50 ng/ml), IL-3 (10 ng/ml), IL-6 (10 ng/ml), and either GM-CSF (10 ng/ml), FLT3 ligand (50 ng/ml or 100 ng/ml), or a combination of both (all from Peprotech). Alternatively, MethoCult (M3334) supplemented with SCF (50 ng/ml), IL-3 (10 ng/ml), IL-6 (10 ng/ml), and erythropoietin (3 U/ml) was used. Individual colonies (defined as containing more than 50 cells) were scored with an inverted light microscope 7–10 days after plating. For the examination of morphology, cells were centrifuged onto glass slides and stained with May-Grunwald-Giemsa, as described before (Fogg et al., 2006).

Progenitor Transplantation Assays

For progenitor transplantation assays, 25,000 flow-sorted progenitors (*Irf8*$^{VENUS+}$ MPs, *Irf8*$^{VENUS-}$ MPs or CDPs, all CD45.2^{+}) were transferred intravenously into sublethally irradiated (6 Gy) 4-week-old recipient mice and analyzed 11 days later or, alternatively, were transferred intravenously into nonirradiated 4-week-old recipient mice (CD45.1^{+}) and analyzed after 7 days.

Microarrays

Lin^{-}IL7Rα^{-}Sca1^{-}ckit^{+}M-CSFR^{+} progenitors were sorted from BM of three independent pools of *Irf8*$^{+/+}$ and *Irf8*$^{-/-}$ mice, respectively. Every pool consisted of cells from three to four animals at the age of 8–12 weeks. Additionally, monocytes and macrophages (CD11b^{+}Ly6C^{+}M-CSFR^{+}), neutrophils (CD11b^{+}Ly6C^{+}M-CSFR^{-}), and total DCs (CD19^{-}CD3e^{-}CD11c^{+}) were sorted from the spleens of three independent pools of C57Bl/6 WT mice, each consisting of three animals at the age of 8–12 weeks. RNA was extracted according to the RNeasy Micro Kit (QIAGEN) protocol. High-quality RNA (Rin > 8.9) was assessed by employing the Agilent 2100 Bioanalyzer. For linear amplification of RNA, a strategy of two rounds of reverse transcription followed by T7 promoter-dependent in vitro transcription was applied with the Ovation Pico WTA System (NuGEN) according to manufacturer's instructions. For each sample, 10 μg of amplified RNA sample was labeled and hybridized in triplicate to a 24-slide cartridge Affymetrix Mouse Genome 430 2.0 Array according to the manufacturer's instructions.

Chromatin Immunoprecipitation

Chromatin immunoprecipitation (ChIP) was performed employing the Low-Cell# ChIP Kit (Diagenode). The antibodies used in this study included anti-PU.1 (T-21X, Santa Cruz Biotechnology), anti-IgG (Millipore, 12-370), and anti-acetyl-histone H3 (Millipore, 06-599). Immunoprecipitates were quantified with SYBR Green quantitative PCR (qPCR) on a 7300 Real-Time PCR System (Applied Biosystems). Results were calculated as percentage of the input sample, and nonspecific IgG control is shown. Primer sequences are available upon request.

Chromosome Conformation Capturing

3C was essentially conducted according to Dekker et al. (2002). In brief, chromatin of 1 × 10^{7} cells was crosslinked by a 10 min treatment with 5.4% formaldehyde followed by quenching with glycine and digestion with *Nco*I (New England Biolabs; 800 U, treated overnight). A fraction was removed as a no-ligation control; the remaining sample was diluted 45 times and religated with T4 DNA Ligase (NE Biolabs). For the analysis of ex vivo populations 1 × 10^{5} flow-sorted progenitor cells, we applied a protocol by Dostie and Dekker (2007) and made minor modifications according to Staber et al. (2013). 3C material was analyzed by nested PCR or by qPCR with a TaqMan probe spanning the *Nco*I site between the Irf8promoter fragment and the −50kb enhancer. Relative crosslinking frequencies were calculated after normalization to total DNA content as quantified at the −50 kb enhancer site. Additionally, relative crosslinking frequencies were calculated after normalization to chromosomal looping at the Gapdh locus, as described before (Spilianakis et al., 2005). qPCR reactions were performed in triplicate and each experiment was repeated independently up to three times. Primers and probes were validated employing the digested and religated *Irf8*-PAC DNA. Digestion efficiency was calculated as in Hagège et al., (2007). Only samples with digestion efficiency > 90% were used. Sequences are available upon request.

Cell Transfections and Luciferase Assays

Stably transformed reporter cell lines were generated by electroporation in RAW264.7 and NIH 3T3 cells with a Gene Pulser Xcell (Bio-Rad). *Pvu*I-linearized reporter plasmids were coelectroporated with a plasmid carrying a puromycin resistance gene. The cells were subsequently kept under puromycin selection for 3 weeks. For the expression of firefly luciferase, 5 × 10^{5} cells of stably transformed pools or single clones were analyzed with the Dual-Luciferase Reporter Assay System (Promega) according to the recommendations of the manufacturer.

RAW264.7 cells were transfected with shRNA-GFP constructs (see Supplemental Information). GFP^{+} cells were sorted 48 hr after transfection, and 5 × 10^{5} cells were analyzed with the Dual-Luciferase Reporter Assay System.

Statistical Analysis

Unpaired Student's t test was carried out to determine the statistical significance of experimental results. All experiments shown were replicated at least two to three times with similar results, unless indicated differently in the figure legends.

ACCESSION NUMBERS

Microarray data have been deposited in the Gene Expression Omnibus (GEO) at accession number GSE45467. For microarray data processing, see Supplemental Information.

SUPPLEMENTAL INFORMATION

Supplemental Information includes Extended Experimental Procedures, six figures, and five tables and can be found with this article online at http://dx.doi.org/10.1016/j.celrep.2013.04.007.

LICENSING INFORMATION

This is an open-access article distributed under the terms of the Creative Commons Attribution-NonCommercial-No Derivative Works License, which permits non-commercial use, distribution, and reproduction in any medium, provided the original author and source are credited.

ACKNOWLEDGMENTS

We thank V. Malchin, N. Endruhn, V. Gröning, M. Käse, and A. Schenk for technical assistance; T. Schröder for plasmids; S. Jung for *Cx3cr1*^{GFP} mice; and M. Feuerer for suggestions on the manuscript. This work was supported by grants from the Helmholtz Association of German Research Centers to F.R., the Helmholtz Alliance on Systems Biology to M.A.A.-N., the Deutsche Forschungsgemeinschaft Priority program 1463 to F.R. and M.A.A.-N, the Deutsche Forschungsgemeinschaft Research Unit 1336 to J.P. and F.R., the Deutsche Krebshilfe to C.S. and F.R., and the Deutsche Jose Carreras's Stiftung to C.S. J.S., C.K., P.R., M.S. and G.H. conducted experiments. M.L.G. and M.A.A.-N. performed computational analyses. F.F.K. and J.P. performed immunohistochemistry. R.N. injected the transgenic constructs into fertilized eggs. A.L. and C.S. provided essential experimental support. F.R. and J.S. wrote the manuscript. F.R. designed and supervised the project. All authors made comments on the manuscript.

Received: May 14, 2012
Revised: November 23, 2012
Accepted: April 8, 2013
Published: April 25, 2013

REFERENCES

Apostolou, E., and Thanos, D. (2008). Virus Infection Induces NF-kappaB-dependent interchromosomal associations mediating monoallelic IFN-beta gene expression. Cell *134*, 85–96.

Becker, A.M., Michael, D.G., Satpathy, A.T., Sciammas, R., Singh, H., and Bhattacharya, D. (2012). IRF-8 extinguishes neutrophil production and promotes dendritic cell lineage commitment in both myeloid and lymphoid mouse progenitors. Blood *119*, 2003–2012.

Bulger, M., and Groudine, M. (2011). Functional and mechanistic diversity of distal transcription enhancers. Cell *144*, 327–339.

Carotta, S., Dakic, A., D'Amico, A., Pang, S.H., Greig, K.T., Nutt, S.L., and Wu, L. (2010). The transcription factor PU.1 controls dendritic cell development and Flt3 cytokine receptor expression in a dose-dependent manner. Immunity *32*, 628–641.

Cisse, B., Caton, M.L., Lehner, M., Maeda, T., Scheu, S., Locksley, R., Holmberg, D., Zweier, C., den Hollander, N.S., Kant, S.G., et al. (2008). Transcription factor E2-2 is an essential and specific regulator of plasmacytoid dendritic cell development. Cell *135*, 37–48.

Dekker, J., Rippe, K., Dekker, M., and Kleckner, N. (2002). Capturing chromosome conformation. Science *295*, 1306–1311.

Dostie, J., and Dekker, J. (2007). Mapping networks of physical interactions between genomic elements using 5C technology. Nat. Protoc. *2*, 988–1002.

Fogg, D.K., Sibon, C., Miled, C., Jung, S., Aucouturier, P., Littman, D.R., Cumano, A., and Geissmann, F. (2006). A clonogenic bone marrow progenitor specific for macrophages and dendritic cells. Science *311*, 83–87.

Geissmann, F., Manz, M.G., Jung, S., Sieweke, M.H., Merad, M., and Ley, K. (2010). Development of monocytes, macrophages, and dendritic cells. Science *327*, 656–661.

Ginhoux, F., Liu, K., Helft, J., Bogunovic, M., Greter, M., Hashimoto, D., Price, J., Yin, N., Bromberg, J., Lira, S.A., et al. (2009). The origin and development of nonlymphoid tissue CD103+ DCs. J. Exp. Med. *206*, 3115–3130.

Guerriero, A., Langmuir, P.B., Spain, L.M., and Scott, E.W. (2000). PU.1 is required for myeloid-derived but not lymphoid-derived dendritic cells. Blood *95*, 879–885.

Hacker, C., Kirsch, R.D., Ju, X.S., Hieronymus, T., Gust, T.C., Kuhl, C., Jorgas, T., Kurz, S.M., Rose-John, S., Yokota, Y., and Zenke, M. (2003). Transcriptional profiling identifies Id2 function in dendritic cell development. Nat. Immunol. *4*, 380–386.

Hagège, H., Klous, P., Braem, C., Splinter, E., Dekker, J., Cathala, G., de Laat, W., and Forné, T. (2007). Quantitative analysis of chromosome conformation capture assays (3C-qPCR). Nat. Protoc. *2*, 1722–1733.

Hambleton, S., Salem, S., Bustamante, J., Bigley, V., Boisson-Dupuis, S., Azevedo, J., Fortin, A., Haniffa, M., Ceron-Gutierrez, L., Bacon, C.M., et al. (2011). IRF8 mutations and human dendritic-cell immunodeficiency. N. Engl. J. Med. *365*, 127–138.

Heermann, D.W. (2011). Physical nuclear organization: loops and entropy. Curr. Opin. Cell Biol. *23*, 332–337.

Heinz, S., Benner, C., Spann, N., Bertolino, E., Lin, Y.C., Laslo, P., Cheng, J.X., Murre, C., Singh, H., and Glass, C.K. (2010). Simple combinations of lineage-determining transcription factors prime cis-regulatory elements required for macrophage and B cell identities. Mol. Cell *38*, 576–589.

Hildner, K., Edelson, B.T., Purtha, W.E., Diamond, M., Matsushita, H., Kohyama, M., Calderon, B., Schraml, B.U., Unanue, E.R., Diamond, M.S., et al. (2008). Batf3 deficiency reveals a critical role for CD8alpha+ dendritic cells in cytotoxic T cell immunity. Science *322*, 1097–1100.

Holtschke, T., Löhler, J., Kanno, Y., Fehr, T., Giese, N., Rosenbauer, F., Lou, J., Knobeloch, K.P., Gabriele, L., Waring, J.F., et al. (1996). Immunodeficiency and chronic myelogenous leukemia-like syndrome in mice with a targeted mutation of the ICSBP gene. Cell *87*, 307–317.

Hume, D.A. (2008). Differentiation and heterogeneity in the mononuclear phagocyte system. Mucosal Immunol. *1*, 432–441.

Jung, S., Aliberti, J., Graemmel, P., Sunshine, M.J., Kreutzberg, G.W., Sher, A., and Littman, D.R. (2000). Analysis of fractalkine receptor CX(3)CR1 function by targeted deletion and green fluorescent protein reporter gene insertion. Mol. Cell. Biol. *20*, 4106–4114.

Kushwah, R., and Hu, J. (2011). Complexity of dendritic cell subsets and their function in the host immune system. Immunology *133*, 409–419.

la Sala, A., He, J., Laricchia-Robbio, L., Gorini, S., Iwasaki, A., Braun, M., Yap, G.S., Sher, A., Ozato, K., and Kelsall, B.; la. (2009). Cholera toxin inhibits IL-12 production and CD8alpha+ dendritic cell differentiation by cAMP-mediated inhibition of IRF8 function. J. Exp. Med. *206*, 1227–1235.

Leddin, M., Perrod, C., Hoogenkamp, M., Ghani, S., Assi, S., Heinz, S., Wilson, N.K., Follows, G., Schönheit, J., Vockentanz, L., et al. (2011). Two distinct auto-regulatory loops operate at the PU.1 locus in B cells and myeloid cells. Blood *117*, 2827–2838.

Ling, J.Q., Li, T., Hu, J.F., Vu, T.H., Chen, H.L., Qiu, X.W., Cherry, A.M., and Hoffman, A.R. (2006). CTCF mediates interchromosomal colocalization between Igf2/H19 and Wsb1/Nf1. Science *312*, 269–272.

Liu, K., and Nussenzweig, M.C. (2010). Origin and development of dendritic cells. Immunol. Rev. *234*, 45–54.

Liu, K., Victora, G.D., Schwickert, T.A., Guermonprez, P., Meredith, M.M., Yao, K., Chu, F.F., Randolph, G.J., Rudensky, A.Y., and Nussenzweig, M. (2009). In vivo analysis of dendritic cell development and homeostasis. Science *324*, 392–397.

Manz, M.G., Traver, D., Akashi, K., Merad, M., Miyamoto, T., Engleman, E.G., and Weissman, I.L. (2001). Dendritic cell development from common myeloid progenitors. Ann. N Y Acad. Sci. *938*, 167–173, discussion 173–174.

Merad, M., and Manz, M.G. (2009). Dendritic cell homeostasis. Blood *113*, 3418–3427.

Onai, N., Obata-Onai, A., Schmid, M.A., Ohteki, T., Jarrossay, D., and Manz, M.G. (2007). Identification of clonogenic common Flt3+M-CSFR+ plasmacytoid and conventional dendritic cell progenitors in mouse bone marrow. Nat. Immunol. *8*, 1207–1216.

Palstra, R.J., Tolhuis, B., Splinter, E., Nijmeijer, R., Grosveld, F., and de Laat, W. (2003). The beta-globin nuclear compartment in development and erythroid differentiation. Nat. Genet. *35*, 190–194.

Rosenbauer, F., Wagner, K., Kutok, J.L., Iwasaki, H., Le Beau, M.M., Okuno, Y., Akashi, K., Fiering, S., and Tenen, D.G. (2004). Acute myeloid leukemia induced by graded reduction of a lineage-specific transcription factor, PU.1. Nat. Genet. *36*, 624–630.

Schiavoni, G., Mattei, F., Sestili, P., Borghi, P., Venditti, M., Morse, H.C., 3rd, Belardelli, F., and Gabriele, L. (2002). ICSBP is essential for the development of mouse type I interferon-producing cells and for the generation and activation of CD8alpha(+) dendritic cells. J. Exp. Med. *196*, 1415–1425.

Schotte, R., Nagasawa, M., Weijer, K., Spits, H., and Blom, B. (2004). The ETS transcription factor Spi-B is required for human plasmacytoid dendritic cell development. J. Exp. Med. *200*, 1503–1509.

Schwenk, F., Baron, U., and Rajewsky, K. (1995). A cre-transgenic mouse strain for the ubiquitous deletion of loxP-flanked gene segments including deletion in germ cells. Nucleic Acids Res. *23*, 5080–5081.

Spilianakis, C.G., Lalioti, M.D., Town, T., Lee, G.R., and Flavell, R.A. (2005). Interchromosomal associations between alternatively expressed loci. Nature *435*, 637–645.

Staber, P.B., Zhang, P., Ye, M., Welner, R.S., Nombela-Arrieta, C., Bach, C., Kerenyi, M., Bartholdy, B.A., Zhang, H., Alberich-Jordà, M., et al. (2013). Sustained PU.1 Levels Balance Cell-Cycle Regulators to Prevent Exhaustion of Adult Hematopoietic Stem Cells. Mol. Cell *49*, 934–946.

Steinman, R.M., and Cohn, Z.A. (1973). Identification of a novel cell type in peripheral lymphoid organs of mice. I. Morphology, quantitation, tissue distribution. J. Exp. Med. *137*, 1142–1162.

Su, H., Mills, A.A., Wang, X., and Bradley, A. (2002). A targeted X-linked CMV-Cre line. Genesis *32*, 187–188.

Tolhuis, B., Palstra, R.J., Splinter, E., Grosveld, F., and de Laat, W. (2002). Looping and interaction between hypersensitive sites in the active beta-globin locus. Mol. Cell *10*, 1453–1465.

Tsujimura, H., Nagamura-Inoue, T., Tamura, T., and Ozato, K. (2002). IFN consensus sequence binding protein/IFN regulatory factor-8 guides bone marrow progenitor cells toward the macrophage lineage. J. Immunol. *169*, 1261–1269.

Tsujimura, H., Tamura, T., Gongora, C., Aliberti, J., Reis e Sousa, C., Sher, A., and Ozato, K. (2003a). ICSBP/IRF-8 retrovirus transduction rescues dendritic cell development in vitro. Blood *101*, 961–969.

Tsujimura, H., Tamura, T., and Ozato, K. (2003b). Cutting edge: IFN consensus sequence binding protein/IFN regulatory factor 8 drives the development of type I IFN-producing plasmacytoid dendritic cells. J. Immunol. *170*, 1131–1135.

Walsh, J.C., DeKoter, R.P., Lee, H.J., Smith, E.D., Lancki, D.W., Gurish, M.F., Friend, D.S., Stevens, R.L., Anastasi, J., and Singh, H. (2002). Cooperative and antagonistic interplay between PU.1 and GATA-2 in the specification of myeloid cell fates. Immunity *17*, 665–676.

Waskow, C., Liu, K., Darrasse-Jèze, G., Guermonprez, P., Ginhoux, F., Merad, M., Shengelia, T., Yao, K., and Nussenzweig, M. (2008). The receptor tyrosine kinase Flt3 is required for dendritic cell development in peripheral lymphoid tissues. Nat. Immunol. *9*, 676–683.

Watowich, S.S., and Liu, Y.J. (2010). Mechanisms regulating dendritic cell specification and development. Immunol. Rev. *238*, 76–92.

Wittkopp, P.J., and Kalay, G. (2012). Cis-regulatory elements: molecular mechanisms and evolutionary processes underlying divergence. Nat. Rev. Genet. *13*, 59–69.